

MITI: SLAM Benchmark for Laparoscopic Surgery

Regine Hartwig^{1,3}, Daniel Ostler¹, Jean-Claude Rosenthal²
Hubertus Feußner¹, Dirk Wilhelm¹, Dirk Wollherr³

Abstract—We propose a new benchmark for evaluating stereoscopic visual-inertial computer vision algorithms (SLAM/ SfM/ 3D Reconstruction/ Visual-Inertial Odometry) for minimally invasive surgical (MIS) interventions in the abdomen. Our MITI Dataset [1] provides all the necessary data by a complete recording of a handheld surgical intervention at Research Hospital Rechts der Isar of TUM. It contains multimodal sensor information from IMU, stereoscopic video, and infrared (IR) tracking as ground truth for evaluation. Furthermore, calibration for the stereoscope, accelerometer, magnetometer, the rigid transformations in the sensor setup, and time-offsets are available. We wisely chose a suitable intervention that contains very few cutting and tissue deformation and shows a full scan of the abdomen with a handheld camera such that it is ideal for testing SLAM algorithms. Intending to promote the progress of visual-inertial algorithms designed for MIS application, we hope that our clinical training dataset helps and enables researchers to enhance algorithms.

I. NOTATION

The following notions are adapted from [2–4] using the rotation groups $SO(3)$ and the rigid motion group $SE(3)$, which fulfill the properties of a Lie group. We use the notation $\exp : \mathfrak{m} \rightarrow \mathcal{M}$ to denote the mapping from tangent space, i.e. Lie algebra \mathfrak{m} to Lie group \mathcal{M} . The Lie algebra $\mathfrak{so}(3) = \text{skew}(3)$ of $SO(3)$ has $d=3$ degrees of freedom and $\mathfrak{se}(3)$, tangent space of $SE(3)$, has $d=6$ degrees of freedom. They are isometric isomorph to \mathbb{R}^d , and we use the function Exp as the composition of the hat operator and the matrix exponential \exp . The function can explicitly be given in closed form by the Rodriguez formula. The inverse mapping is denoted by Log , which is the mapping from the Lie-Group to \mathbb{R}^d . We further use the $\ominus : \mathcal{M} \times \mathcal{M} \rightarrow \mathbb{R}^d$ as

$$\mathbf{T}_1 \ominus \mathbf{T}_2 := \text{Log}(\mathbf{T}_1^{-1} \mathbf{T}_2). \quad (1)$$

II. DATASET

In this section, we introduce our dataset and calibration procedures. It contains data from the MIS use case, which we make publicly available at [1]. In Fig. 1 we show the sensor setup during the data acquisition process.

The sensor data consists firstly of stereoscopic RGB images from the view inside the abdomen. Secondly, it contains two 9DOF IMU sensor data (Angular Velocity, Acceleration, Magnetic Field). One sensor additionally sends the internally computed orientation information w.r.t. a world frame. Both

sensor boards are attached to the laparoscope handle. Thirdly, an IR tracking camera that emits invisible infrared light to the scene detects reflecting passive spheres. This sensor provides poses (orientation and position) for two targets, each consisting of 3-4 passive spheres arranged in a rigid, distinguishable geometry. The individual sensor-data streams are described in more detail in Subsection II-A.

To explain the poses of the individual capturing devices to one another and to define the calibration data, in Subsection II-B we assign names to coordinate systems used throughout this paper and in the dataset.

A. Sensor Setup

- Karl Storz 3D Tipcam Image1 S, 30 degree, 10mm diameter (26605BA)
 - 59,9Hz 1080p RGB stereointerlaced signal
- Metawear MetamotionR 9DOF IMU Sensorboard
 - 220Hz Gyroskop, Accelerometer, Quaternions
- Metawear MetamotionR 9DOF IMU Sensorboard
 - 220Hz Gyroskop, Accelerometer, Magnetometer
- NDI Polaris Vega
 - 20Hz Position + Quaternion to 2 separate targets with passive spheres

B. Coordinate Systems

We now introduce the coordinate systems describing our data shown in Fig. 2. The world coordinate systems are $WIMU0$, $WIMU1$ and WIR for the different sensor modalities. The IMUs are located at $LIMU0$ and $LIMU1$ while L and $W2$ are the poses of infrared targets consisting of passive spheres.

We attach L , $LIMU0$, $LIMU1$ to the laparoscope handle and $W2$ to the patient to detect movements of the operating table.

The tip of the laparoscope with x-axis aligned with the endoscope, z-axis pointing upwards is $CamTip$, while the



Fig. 1: Data Acquisition (a) IMU sensorboards and IR passive targets attached to stereoscopic laparoscopic camera (b) IR sensor and 3D monitor in the operatingroom

¹Authors are with Research Group MITI, Surgical Department, Technical University of Munich (TUM), Germany

²Authors are with Fraunhofer HHI, Berlin, Germany

³Authors are with Chair of Automatic Control Engineering, Department of Electrical and Computer Engineering, Technical University of Munich (TUM), Germany regine.hartwig@tum.de

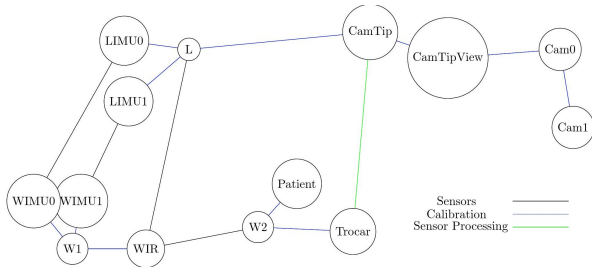


Fig. 2: Coordinate System Naming Convention

coordinate system `CamTipView` represents the 30-degree twist of the lenses, which is typical for laparoscopic interventions. The coordinate system for the left lens is `Cam0` and for the right lens is `Cam1`.

Another essential information or representing the surgical scene is the trocar entry point `Trocar`, which is the pivot and entry point of the camera and is defined to have the same orientation as `W2`.

III. CALIBRATION

We calibrated the camera and the IMU, determining sensor-specific parameters and calculated time offsets using the subsequent models. The calibration parameters can be found in `calibration/* .csv`.

A. Camera Calibration

For camera calibration as described in [5] we captured a checkerboard pattern. A pinhole camera model and a radial distortion function approximate the projection for each lens. The pinhole projection $\Pi_0 : \mathbb{R}^3 \rightarrow \mathbb{R}^2$ from a point $x \in \mathbb{R}^3$ in coordinate system of left `C0` or right `C1` lens to the undistorted image point u_u in the image plane is parameterized by focal lengths f_x, f_y and optical center c_x, c_y both measured in pixel

$$x = \begin{bmatrix} X \\ Y \\ Z \end{bmatrix} \mapsto u_u = \frac{1}{Z} \begin{bmatrix} f_x X \\ f_y Y \end{bmatrix} + \begin{bmatrix} c_x \\ c_y \end{bmatrix}. \quad (2)$$

Radial image distortion is compensated by a low order polynomial model with up to 6 degrees describing the projection from distorted to undistorted image pixels $d : \mathbb{R}^2 \rightarrow \mathbb{R}^2$,

$$u_u = \begin{bmatrix} u_u \\ v_u \end{bmatrix} \mapsto u_d = \begin{bmatrix} u_u(1 + k_1 r^2 + k_2 r^4 + k_3 r^6) \\ v_u(1 + k_1 r^2 + k_2 r^4 + k_3 r^6) \end{bmatrix}. \quad (3)$$

The estimation of k_1, k_2, k_3 is a minimization problem and is computed by a least-square solver. Additionally, the extrinsic parameters are calibrated which determine the orientation between both cameras `C0` and `C1` by a rigid body transformation ${}^c_0T \in SE(3)$. The overall projection function $\Pi(\cdot)$ is a composition of rotation and translation from `CamTip` to `C0` or `C1` and projection from 3D bearing vector to distorted 2D image coordinates by composition of (2) and (3). Fig. 3 shows calibrated sensor readings.

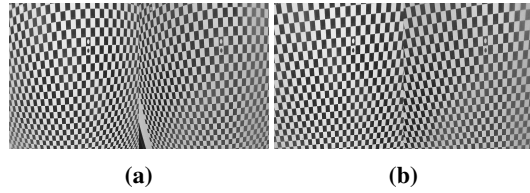


Fig. 3: Calibration Pattern (a) distorted (b) undistorted

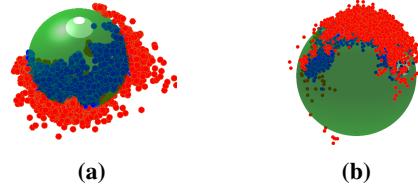


Fig. 4: Calibrated IMU measurements, i.e., red in front, blue behind sphere (a) ${}^c_a - {}^c_g$ in $9.81 \frac{m}{s^2}$ and unit sphere (b) c_m in μT and sphere with radius 48.6

B. IMU Calibration

The accelerometer measurements $\tilde{a}(t)$ are modeled as

$$\tilde{a}(t) = (a(t) - g(t))d_a^{-1} + n_a(t) + b_a \quad (4)$$

with acceleration $a(t) \in \mathbb{R}^3$, gravity $g(t) \in \mathbb{R}^3$, errors $b_a \in \mathbb{R}^3$, $d_a \in \mathbb{R}$ and $n_a(t) \sim \mathcal{N}(0, \sigma_a^2 \mathbf{I})$. We optimize the sum over all measurements

$$\min_{d_a, b_a} \sum_i (g^2 - \|\tilde{a}(t_i) - b_a\| d_a)^2, \quad (5)$$

with

$$g = \|g(t)\| = 9.81 \frac{m}{s^2}$$

and assuming constant velocity s.t. $a(t) = 0$. Furthermore we model the error of magnetometer readings $\tilde{m}(t)$ by

$$\tilde{m}(t) = m(t)d_m^{-1} + n_m(t) + b_m, \quad (6)$$

with magnetic field strength $m(t) \in \mathbb{R}^3$, errors $b_m \in \mathbb{R}^3$, $d_m \in \mathbb{R}$ and $n_m(t) \sim \mathcal{N}(0, \sigma_m^2 \mathbf{I})$. The minimization problem is

$$\min_{d_m, b_m} \sum_i (m^2 - \|\tilde{m}(t_i) - b_m\| d_m)^2. \quad (7)$$

The corrected measurements lie on a sphere with radius equal to the strength of the earths magnetic field

$$m = \|m\| = 48.6 \mu T$$

in Munich, Germany. Fig. 4 shows calibrated sensor readings.

C. Timeoffset Calibration

The sensor data has been synchronized during the acquisition process by configuring an NTP server/client at the data receiving devices. Additionally, the remaining offset is minimized by evaluating the tangent for each sensor at coordinate system `CamTip` at time t_i

$${}^c_{\xi} \xi_{t_i} \approx \frac{{}^cT_{t_i + \Delta t} \ominus {}^cT_{t_i}}{\Delta t} \in \mathbb{R}^6. \quad (8)$$

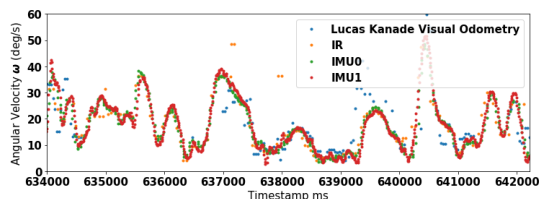


Fig. 5: Time-calibrated angular velocity part $\|c\omega_{t_i}^{(k)}\|$ of different sensor modalities

We calibrate the timeoffset dt by comparing the velocities acquired from different sensors

$$j, k \in \{\text{"Visual Odometry"}, \text{"IR"}, \text{"IMU0"}, \text{"IMU1"}\}.$$

The sum of differences at different timeoffsets

$$\min_{dt} \sum_i \left\| c\xi_{t_i+dt}^{(j)} - c\xi_{t_i}^{(k)} \right\|. \quad (9)$$

Fig. 5 shows the time-calibrated normalized angular velocity part of the different sensor modalities. For that, we determine the camera-based angular velocity using the visual odometry algorithm based on Lucas Kanade feature tracks without IMU and IR.

REFERENCES

- [1] R. Hartwig, D. Ostler, J.-C. Rosenthal, H. Feussner, D. Wilhelm, and D. Wollherr, "Miti: Slam benchmark for laparoscopic surgery," TUM, 2021, login for reviewers is available; username:review-hartwig-sensorfusion; password: 6H-PfFgYnCXz. [Online]. Available: <https://mediatum.ub.tum.de/1621941>
- [2] T. D. Barfoot, *State estimation for robotics*. Cambridge University Press, 2017.
- [3] J. Sola, J. Deray, and D. Atchuthan, "A micro lie theory for state estimation in robotics," *arXiv preprint arXiv:1812.01537*, vol. 5, p. 1371, 2018.
- [4] C. Sommer, V. Usenko, D. Schubert, N. Demmel, and D. Cremers, "Efficient derivative computation for cumulative b-splines on lie groups," in *Proceedings of the IEEE/CVF Conf. on Computer Vision and Pattern Recognition*, 2020, pp. 11 148–11 156.
- [5] Z. Zhang, "A flexible new technique for camera calibration," *IEEE Trans. on pattern analysis and machine intelligence*, vol. 22, no. 11, pp. 1330–1334, 2000.